Femtosecond laser induced nanostructuring of zirconium in liquid confined environment

You may also be interested in:

Femtosecond laser induced nanostructuring of zirconium in liquid confined environment

Nisar Ali[1,2,3,4,†], Shazia Bashir[3], Umm-i-Kalsoom[2,3,4,5], M. Shahid Rafique[6],
Narjis Begum[7], Wolfgang Husinsky[1], Ali Ajami[1], and Chandra S. R. Natahala[1]

[1]*Laser Laboratories, Institute for Applied Physics, Vienna University of Technology, 1040 Vienna, Austria*

[2]*Department of Basic Sciences and Humanities, University of Engineering and Technology Lahore, Faisalabad Campus, Faisalabad, Pakistan*

[3]*Laser Laboratories, Centre for Advanced Studies in Physics, GC University 1-Church Road Lahore, Pakistan*

[4]*Department of Physics, GC University Kachehri Road Lahore, Pakistan*

[5]*Department of Physics, Riphah International University Islamabad (Lahore Campus), Lahore, Pakistan*

[6]*Department of Physics, University of Engineering and Technology Lahore, Pakistan*

[7]*Department of Physics, COMSATS Institute of Information Technology, Islamabad, Pakistan*

The surface, structural, and mechanical properties of zirconium after irradiation with Ti: sapphire laser (800 nm, 30 fs, 1 kHz) have been investigated. The zirconium targets were exposed for a varying number of laser pulses ranging from 500 to 2000 at a fixed fluence of 3.6 J/cm^2 corresponding to an intensity of 1.2×10^{14} W/cm^2 in ambient environments of de-ionized water and propanol. A scanning electron microscope (SEM) was employed to investigate the surface morphology of the irradiated zirconium. The SEM analysis shows the formation of various kinds of features including nanoscale laser induced periodic surface structures (LIPSS), sponge like surface structure, flakes, conical structures, droplets, pores, and cavities. The energy dispersive x-ray spectroscopy (EDS) analysis exhibits the variation in chemical composition along with an enhanced diffusion of oxygen under both ambient conditions. The crystal structure and phase analyses of the exposed targets were explored by x-ray diffraction (XRD) and Raman spectroscopy techniques, respectively. The XRD analysis confirms the presence of various phases of zirconium hydride and zirconia after ablation in both de-ionized water and propanol. However, excessive hydrides are formed in the case of propanol. The Raman analysis supports the EDS and XRD results. It also reveals the presence of oxides (zirconia) after irradiation in both de-ionized water and propanol environments. The chemical reactivity of zirconium was significantly improved in the presence of liquids which were accountable for the growth of novel phases and modification in the chemical composition of the irradiated Zr. A nanohardness tester was employed to measure the nanohardness of the laser treated targets. The initial increase and then decrease in nanohardness was observed with an increase in the number of laser pulses in the de-ionized water environment. In the case of propanol, a continuous decrease in hardness was observed.

Keywords: ambient environments, periodic structure, crystallinity, synthesis

1. Introduction

Femtosecond pulsed laser ablation of materials is a promising technique due to its enormous applications in the field of laser based material processing.[1,2] The laser ablation mechanisms depend upon the laser parameters (number of laser pulses, energy per pulse, pulse width, wavelength, etc.) as well as the ambient conditions and the thermo-physical properties of the target material. Femtosecond laser induced ablation causes the formation of various kinds of nanostructures such as cones, cavities, pores, spherical droplets, etc. on metals, semiconductors, and dielectrics.[3,4] Laser induced periodic surface structures (LIPSS) or ripples are one of the most important features to be found in the surface of the irradiated materials and have been reported by many groups.[5,6] It is also an important technique for the fabrication of various hydride and oxide films grown by the chemical reaction taking place at the liquid–solid interface.[7] Therefore, it is very important to investigate ablation of a variety of metals and metallic alloys in diverse ambient environments. Femtosecond laser ablation of solid materials in liquid environments evokes extensive research interests due to its plentiful advantages and applications in nano fabrication. The development of highly confined plasma pressure, efficient cooling, ease and precise nature makes this technique highly useful and beneficial.[7,8]

Zirconium is a transition metal and has growing applications in the field of industry, e.g., in vacuum tubes, an alloying agent in steel, and as a component in surgical appliances, photoflash bulbs, and various others.[9] Zirconium's thermal conductivity, corrosion resistance, formability, strength, and minimum creep properties under high service temperatures and pressures favor it as a highly suitable and appropriate metal for making crucibles, gas turbines, liners for jets, rocket motor tubes, and high resistance and ultra-high frequency furnaces.[10] The purpose of surface and structural modifica-

---

tion of zirconium by femtosecond laser irradiation is to develop and modify its wide range functional as well as physical, chemical, and mechanical properties such as, hardness, wear and corrosion resistance, etc. The growth of nanostructures on the material surface can improve its optical absorption, thermionic and field emission properties, and hardness.[11,12]

Laser ablation of zirconium in de-ionized water and propanol can introduce various nonlinear effects and enhance the thermal and chemical reactivity at the solid–liquid interface, and therefore tetragonal phase and monoclinic phase of zirconia (ZrO_2) as well as metal-hydrides and metal-hydroxide can be formed. Zirconia (ZrO_2) is a wide band gap (5.0–5.5 eV) transition metal oxide with excellent thermal, mechanical, electrical, and optical properties.[13] It is used as a refractory material in the production of rings of high frequency induction reels, piezoelectric crystals, fuel cells, sensors, etc.[14] Rechargeable hydrides of metal show a wide range of applications: hydrogen purification, stationary and mobile hydrogen storage, recovery of hydrogen and separation, chemical heat pumps, thermal compression and refrigeration.[15] Hydroxides have applications as magnetic materials precursors, additives in polymers, and in biology and medicine.[16] The growth of various structures can be well correlated with the enhancement of the chemical reactivity of zirconium. For this purpose, zirconium targets are ablated with a Ti: sapphire laser for various numbers of laser pulses in an ambient environment of de-ionized water and propanol. Various diagnostic techniques such as scanning electron microscope (SEM), energy dispersive x-ray spectroscopy (EDS), x-ray diffractometry (XRD), raman spectroscopy, and nanohardness techniques are employed to correlate the surface features and nanohardness with the change in the chemical composition and crystallinity after irradiation.

2. Experimental setup

A chirped pulse amplified (CPA) Ti: sapphire laser amplifier seeded from a mode locked Ti: sapphire oscillator was used for the ablation of zirconium targets. The system was operating at the central wavelength of about 800 nm and the repetition rate of 1 kHz with the pulse duration of about 30 fs. The P-polarized beam was focused through a lens of focal length 20 cm. Zirconium targets with dimensions of 8 mm × 8 mm × 2 mm were grinded, polished, and ultrasonically cleaned with acetone for 30 min. The prepared targets were placed in a quartz cuvette of height 45 mm and width 10 mm with the help of a target holder. The schematic of the experimental setup has been shown elsewhere.[17]

For each exposure, the quartz cuvette was filled with fresh liquid. The thickness of the liquid layer above the sample surface was about 4 mm. All samples were irradiated with a laser for a constant laser fluence of 3.6 J/cm^2 and an intensity of 1.2×10^{14} W/cm^2. The numbers of overlapping laser pulses used for the exposure of the targets were 500, 1000, 1500, and 2000. Two sets of experiments were performed for the ambient environments of (i) de-ionized water and (ii) propanol under the same laser parameters.

For the 800 nm wavelength, the percentage laser energy absorption was calculated to be 2.07% for de-ionized water and 2.76% for propanol. By using the following equation of Beer–Lambert law $I(x) = I_0 e^{-\alpha x}$,[18] the absorption coefficient was evaluated for de-ionized water and propanol, which came out to be 7.6×10^{-3} mm^{-1} and 1.02×10^{-2} mm^{-1}, respectively.

The surface morphology of the irradiated zirconium targets was investigated by using SEM (FEI-QUANTA 200F). The EDS analysis was performed for chemical analysis of the irradiated targets. Structural and phase analyses were carried out by using XRD (X'Pert PRO MPD) and micro Raman spectroscopy (DONGWOO OPTRON, MSS-400A). Nanohardness was measured by using a nanohardness tester (CSM instruments, NHT+MHT).

3. Results and discussion

Figure 1 presents the surface morphology of the zirconium samples after irradiation in an ambient environment of de-ionized water for various numbers of laser pulses, i.e., 500, 1000, 1500, and 2000 at a fixed fluence of 3.6 J/cm^2. Figures 1(a)–1(d) present the overall view of the ablated area of the zirconium targets for various numbers of laser pulses. A modified smooth surface morphology with size of ∼ 325 μm × 260 μm is observed after irradiation with 500 laser pulses (Fig. 1(a)). In Figs. 1(b)–1(d), no significant change in the size of the ablated area is observed with the increase in the number of laser pulses up to 2000. However, with 2000 pulses (Fig. 1(d)), the ablated area shows the presence of a large number of self-organized craters with an average spacing of 20 μm.

Figures 1(e)–1(h) reveal the surface morphology of the central ablated area of zirconium after irradiation for various numbers of laser pulses. One large sized cavity along with a large number of pores, non-uniform and incomplete melting of the target is observed with 500 laser pulses (Fig. 1(e)). Figures 1(f)–1(g) show reduced melting and development of laser induced periodic surface structures (LIPSS) with an average periodicity of about 340 nm with an increase in the number of pulses up to 1500. Software Image J was used to measure the average periodicity of LIPSS. The P-polarized light was used to irradiate the targets and LIPSS were formed perpendicular to the E-field. For 2000 laser pulses, LIPSS with an average periodicity of 370 nm are observed (Fig. 1(h)).
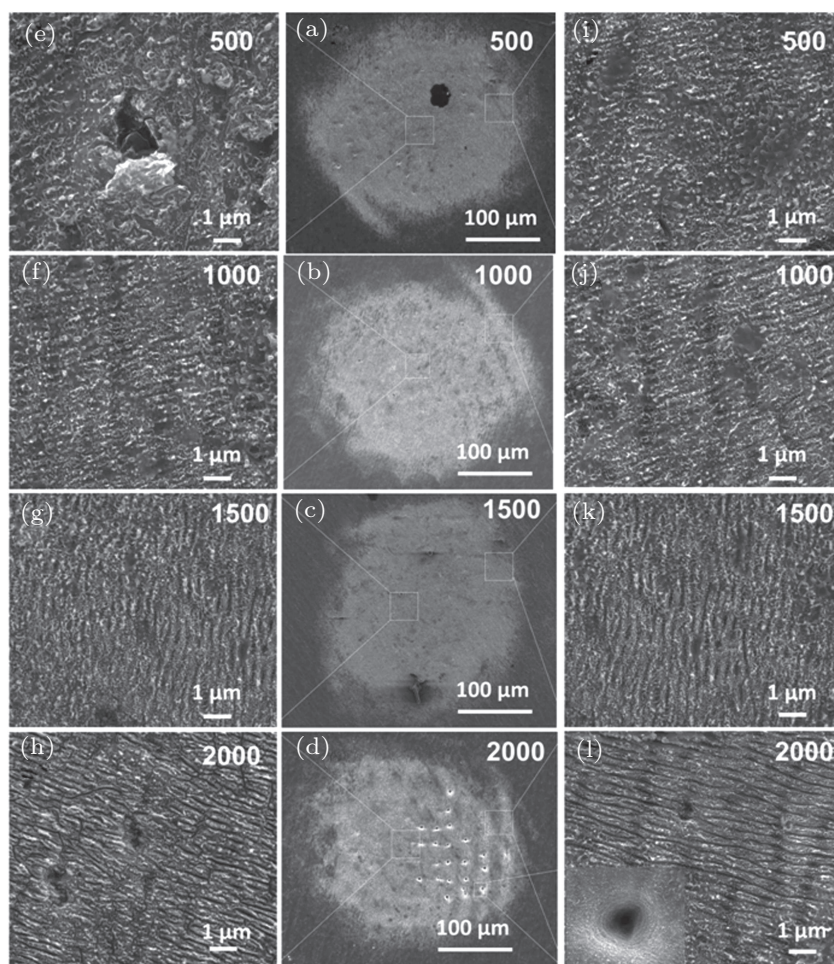
Fig. 1. SEM images revealing the surface morphology of zirconium samples after irradiation in an ambient environment of de-ionized water for various numbers (i.e., 500, 1000, 1500, and 2000) of femtosecond laser pulses at a fixed fluence of 3.6 J/cm^2: (a)–(d) overall ablated area, (e)–(h) magnified central ablated areas, and (i)–(l) magnified peripheral ablated areas.

Figures 1(i)–1(l) reveal the surface morphology of the peripheral ablated area of zirconium for various numbers of laser pulses. Figure 1(i) shows the initial stage of LIPSS formation along with the development of nanocones, pores, cavities and some signs of melting and splashing for 500 laser pulses. An increase in the number of pulses up to 1000 (Fig. 1(j)) leads to LIPSS with an average periodicity of 320 nm along with reduced melting. Further increase in the number of laser pulses up to 2000 results in an increase in the average periodicity of LIPSS upto 380 nm (Fig. 1(l)). The inset of Fig. 1(l) shows the magnified SEM image of the crater with a diameter of 4.34 μm formed at the peripheral ablated area. The crater is surrounded by circular ripples, which vanish at the outskirt of the crater. At the periphery of the crater, the appearance of randomly oriented emerging out branches and globule like structures is observed.

The formation of cavities, splash like structures, and pores on the surface of zirconium after irradiation under the action of compressed plasma flow can be related to violent boiling and bubble formation in the superheated liquid layer. Bubbles burst inside the liquid layer due to the turbulence of the boiling, and the fast cooling leads to the formation of cavities and pores, while the frozen melt gives rise to the splash

like structures. Melting, fast cooling, resolidification, and thermal stresses generated during irradiation are responsible for the crack formation.[19,20] The generation of LIPSS can be explained on the basis of surface plasmons (SP's) theory.[21] Surface plasmon polariton excitation by isolated surface defects and rough surfaces causes the formation of LIPSS after irradiation by multiple laser pulses.[20,22,23] During multipulse irradiation, the first few pulses of the laser enhance the surface roughness of the target material. During the interaction of the laser, a critical density of electrons is close to the sample surface. At normal incidence, the laser electric field (E) would stimulate oscillations parallel to the surface. The laser light will be scattered tangentially to the surface due to surface irregularities, which could produce a standing wave pattern. The combined incident, diffracted, and reflected waves could give an E-field distribution which is capable of driving localized plasma oscillations.[24] This results in dislocation of the material in the form of ridges or ripples.[24]

During the fs laser matter interaction process, in a time regime of tens of femtoseconds, the electrons get excited upto tens of eV[25] by photo ionization and avalanche ionization.[26] While the duration of energy transport from electrons to ions is on the order of picoseconds.[27] Hence, the temperature of

the lattice remains unaffected during the absorption of femtosecond laser pulse. At the start, during the first stage, the surface inhomogeneous fluctuations cause the scattering of the incident laser radiations, which results in excitation of surface EM waves. The interference of the surface EM waves with the incident laser radiation results in the production of a spatially modulated temperature field along the surface. Initially, the seeded modulated temperature is very small, of the value of the e$^-$ temperature (T_e). However, the instability phenomenon occurs between the periodic components of the electron temperature and the absorption of laser pulse in the case of a positive feedback. This results in the creation of a periodically modulated electron temperature distribution that is generally referred to as the "temperature lattice". At the 2nd stage, during thermalization of both the crystal lattice and the electron subsystem, the periodically modulated component of the electrons transfers to the lattice in several ps. The following process of periodic modulation takes place due to melting of the surface layer and its thermal expansion. For normal irradiance, the period of the surface EM waves agrees with the period of modulation that was generated during the 1st stage. The surface tension forces, at this moment, play their role in smoothing the formed liquid in shape of periodic surface structures (LIPPS). The melted surface layer re-solidifies during the 3rd stage. The duration between the 2nd and the 3rd stages is too short to allow the surface tension forces to smooth the surface and one can observe the formation of LIPPS.[28]

Nanoscale LIPSS formation can also be explained on the basis of stimulated Raman scattering (parametric decay model). According to this model, the plasma wave travels slowly at a speed of less than 1% of the speed of light and an ion enriched local area appears. Before the next peak of the electron wave arrives, the ions experience a strong Coulomb repulsive force, causing a Coulomb explosion. Through this process, periodic ripple structures may be formed.

The observed increase in periodicity of LIPSS at both the central and the peripheral ablated areas is attributable to enhanced energy absorption by the zirconium surface with an increasing number of laser pulses.[29] The formation of nanocones and globules is attributable to quick solidification of the melted layer.[30] The formation of circular ripples is due to the formation and expansion of bubbles.[5] There are a number of possible mechanisms by which the bubbles may generate the wave like structures shown in Fig. 2(l). Diffraction of the laser beam by the bubbles may cause rings of light intensity on the metallic surface. The heat of dissociation and vaporization required to form the bubbles at the liquid-metal interface may locally cool the metallic surface, exciting a capillary wave in the molten zirconium through Marangoni flow.[31] The dissociation and vaporization eliminate thermal energy from the molten surface just underneath the bubble, causing it to rapidly cool. The increase of temperature causes a decrease in the surface tension and the surrounding hot liquid

starts flowing towards the cooled region, resulting in deformation of the surface.[4] This deformation results in circular capillary waves. After multipulse irradiation, superposition of the capillary waves causes organized periodic surface structures. Hydrodynamic instabilities at the solid–liquid interface due to interaction of accumulative laser pulses also play a considerable role for the formation of ripples and cavities.[4]

Figure 2 reveals the surface morphology of the zirconium samples after irradiation in an ambient environment of propanol for various numbers of laser pulses, i.e., 500, 1000, 1500, and 2000 at a fixed fluence of 3.6 J/cm^2. Figures 2(a)–2(d) present the overall view of the ablated zirconium targets. Figure 2(a) shows a wavy shaped modified morphology with size of $\sim$300 μm$\times$ 260 μm with no significant redeposited material across the periphery. An increase in the number of pulses up to 1500 (Fig. 2(c)) leads to some randomly distributed craters with no effect on the size of the ablated area. An increase in the number density of randomly distributed craters is observed with an increase in the number of laser pulses up to 2000 (Fig. 2(d)) again with no effect on the size of the ablated area. The measured percentage energy loss in propanol (2.76%) is more than that in de-ionized water (2.07%), which may be a reason for the wavy shaped morphology of the ablated area. The wavy shaped modified morphology can also be attributable to the formation of excessive hydrides in propanol as compared to de-ionized water.[17]

Figures 2(e)–2(h) reveal the magnified surface morphology of the central ablated area of the zirconium targets. Figure 2(e) shows a non-uniform distribution of the sponge like surface structure along with cones, cracks, and some signs of melting for 500 laser pulses. For 1000 pulses, an increase in the density of cracks but a decrease in the size of nanopores and the number density of cones is observed (Fig. 2(f)). A further increase in the number of laser pulses up to 2000 (Fig. 2(h)) results in an increase in the number density of pores. However, a decrease in the size and the number density of cracks and nanocavities is observed due to enhanced melting.[5]

Figures 2(i)–2(l) show the magnified surface morphology of the peripheral ablated area of zirconium for various numbers of laser pulses. Structures formation is not observed at the peripheral ablated areas. It only shows cavities, cracks, and flake like structures which are attributable to exfoliational sputtering. Increasing the number of laser pulses shows no significant change in the surface morphology of the ablated area. The inset of Fig. 2(l) shows the magnified image of the crater with a diameter of 4.87 μm formed after irradiation in propanol environment. This crater is surrounded by circular ripples whose periodicity decreases towards the outskirt of the crater. At the periphery of the crater, these ripples completely vanish with an appearance of randomly oriented emerging out branches and globule like structures and cracks.
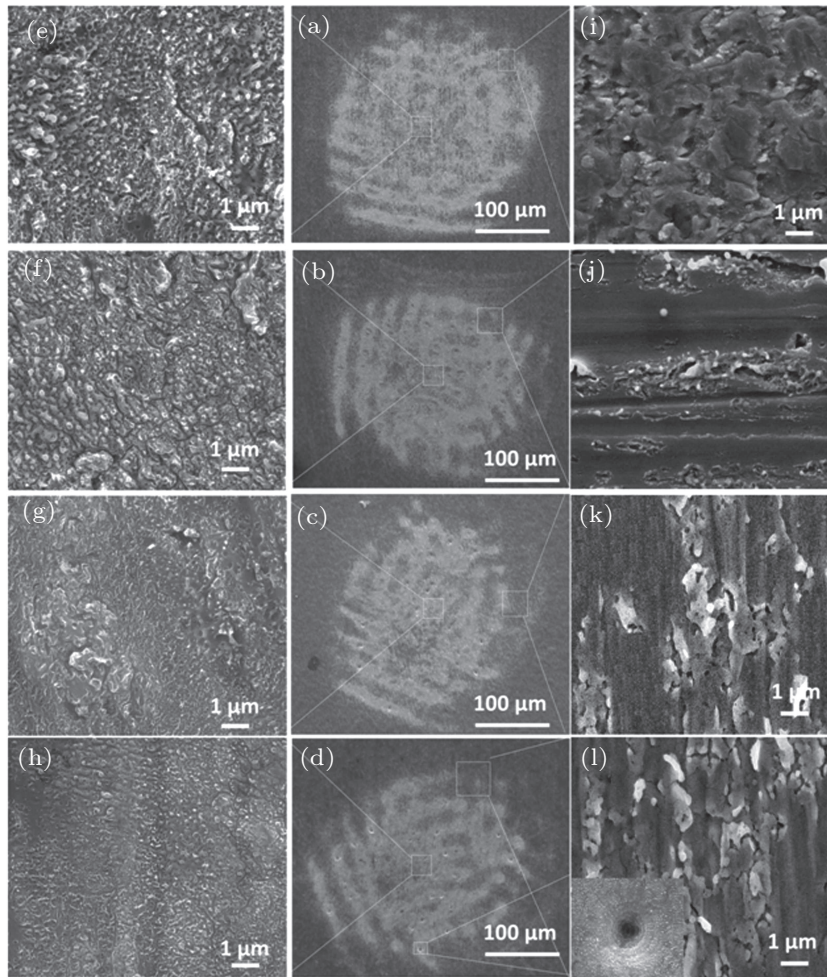
Fig. 2. SEM images revealing the surface morphology of zirconium samples after irradiation in an ambient environment of propanol for various numbers (i.e., 500, 1000, 1500, and 2000) of femtosecond laser pulses at a fixed fluence of 3.6 J/cm^2: (a)–(d) overall ablated area, (e)–(h) magnified central ablated areas, and (i)–(l) magnified peripheral ablated areas.

A comparison of both ambient environments shows significant dissimilarities in the surface morphology of the ablated zirconium. The surface morphologies of the craters produced in de-ionized water are much smoother than those in propanol, which might be due to the different interacting mechanisms, such as recoil pressures, production of bubbles, the absorption coefficient, and the difference in the boiling point of the two liquids.

During ablation in the de-ionized water environment, the appearance of the ablated area is smooth, whereas, after ablation in the propanol environment, a wavy shaped modified morphology of the ablated area is observed. In the case of ablation in de-ionized water, LIPSS are observed at both the central and the peripheral ablated areas along with some bifurcations such as pores, cavities, and cracks. While, in the case of a propanol environment, a sponge like surface structure, cones, cracks, and cavities appear. No LIPSS are seen after irradiation in propanol. These results confirm that de-ionized water is more supportive for the growth of LIPSS.

In this study, the liquid (de-ionized water and propanol) has played a considerable role in confining the plasma and cooling the ablated target. Quick rise in temperature during plasma formation and expansion generates cavitation bubbles in the liquid environment. The bubble formation would be accompanied with shock waves, which will provide an extra source or force to clean off the debris produced by the laser ablation.[13] The improved mechanical wave emission assists the removal of the laser ablated materials and also offers a considerable photomechanical effect and pressure impact on the target. The laser ablation in a liquid confined environment can enhance the efficiency of material ablation in terms of nano-structuring by means of explosive vaporization of liquid in association with the mechanical impact on the target.

Chemical analysis of the pristine and the femtosecond laser irradiated zirconium targets at a laser fluence of 3.6 J/cm^2 under ambient environments of de-ionized water and propanol is illustrated in Table 1. A decrease in the content of zirconium but an increase in the content of oxygen is observed after irradiation in both ambient environments. The recoil pressure of the laser-induced plasma enhances the diffusion of oxygen atoms to the surface of zirconium due to the adsorption of atomic oxygen.[32] Therefore, the irradiated targets carry

more oxygen content.

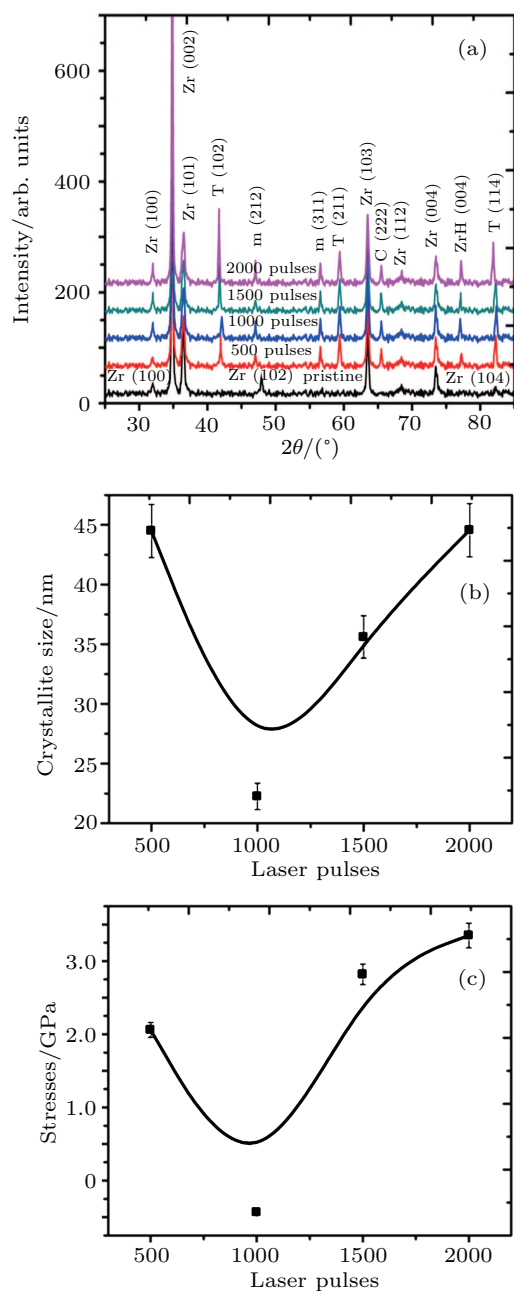| Elements	Untreated	De-ionized water	propanol
Zr/wt.%	87.52	76.67	84.02
B/wt.%	2.78	2.63	1.02
C/wt.%	2.82	2.59	2.51
O/wt.%	4.91	15.55	11.03
Re/wt.%	1.97	2.56	1.42

Fig. 3. (color online) (a) XRD patterns of the pristine and the femtosecond laser irradiated zirconium exposed to various numbers of laser pulses at a fixed fluence of 3.6 J/cm² under ambient environment of de-ionized water. (b) The variation in the crystallite size and (c) the variation in stresses for varying pulses.

In order to investigate the structural changes in the ab-

lated zirconium, XRD analysis was carried out. Figure 3(a) shows the XRD of the pristine and the laser irradiated zirconium exposed to various numbers of laser pulses under an ambient environment of de-ionized water. In the case of pristine zirconium, hexagonal phases of Zr (100), (002), (101), (102), (110), (103), (112), (004), and (104) (pattern No. 01-089-3045) are identified. New phases of zirconium oxide (tetragonal): ZrO_2 (102), (211), (114); monoclinic: ZrO_2 (212), (311); cubic: ZrO_2 (222) and zirconium hydride: ZrH (004) are observed along with the original phases of zirconium.

Figure 3(b) shows the variation in the crystallite size of ZrO_2 (102) plane reflection as a function of laser pulses. Figure 3(c) presents the variation in the residual stresses with an increasing number of laser pulses.

The crystallite size is evaluated for ZrO_2 (102) plane reflection by using Scherrer's formula.[33] The residual strains are evaluated by using the following relation $\varepsilon = (d - d_0)/d_0$,[33] where ε is the induced strain, d_0 is the standard plane spacing, and d is the observed plane spacing. The induced stresses are calculated by using the relation $\sigma = \varepsilon E$, where ε is the induced strain, E is the Young modulus, and its value is 248 GPa for ZrO_2 at 20 °C.[34]

The peak intensity (Fig. 3(a)) and the crystallite size (Fig. 3(b)) decrease with an increase in the number of laser pulses up to 1000. A further increase in the number of laser pulses up to 2000 results in a continuous increase in the peak intensity and the crystallite size of ZrO_2 (102) plane reflection. The initial decrease in the peak intensity and the crystallite size is attributable to interstitial diffusion of oxygen atoms/ions. The interstitial diffusion of oxygen atoms/ions induces microstrain defects and these induced defects cause an increase in FWHM and reduction in the peak intensity and the crystallite size.[17] The increase in the peak intensity and the crystallite size with further increase in the number of pulses is due to the maximum diffusion of oxygen atoms across the grain boundaries[35] and enhancement diffraction of x-rays from the target.[36]

Variation in the residual stresses with an increase in the number of laser pulses is depicted in Fig. 3(c). Laser induced thermal shocks and lattice defects generated by oxygen ions incorporation into the lattice may cause the residual stress variation. Laser induced thermal shock causes the tensile stresses whereas oxygen ion implantation results in the compressive stresses.[37] The thermal shock induced tensile residual stresses are dominant for 500 laser pulses, which relax and transform to compressive stresses on increasing the number of pulses up to 1000. The relaxation in the tensile residual stresses and their transformation to the compressive stresses are due to the reduction in the crystallite size. Diffusion of oxygen atoms into the surface causes the decrease in the crystallite size and hence causes the highly tensile stresses to relax

and transform into the compressive residual stresses.[17] The peak shift to a higher angular position confirms the relaxation and transformation of the tensile residual stresses to the compressive stresses.[38] A further increase in the number of laser pulses up to 2000 results in increasing tensile stresses. This relaxation of the compressive stresses and their transformation into the tensile stresses with an increase in the number of laser pulses are attributable to the laser induced thermal shock or it may be due to the increased crystallite size caused by the atomic diffusion across the grain boundaries.[37] The peak shift to lower angular position is also evident for the transformation of compressive to tensile residual stresses. Melting of the target and ionization of the ambient gas take place during irradiation, which increase the reaction rate between the molten layers of the target and atomic oxygen. This reaction during the resolidification causes the formation of several new phases of oxides of zirconium.[39] These results are well correlated with the SEM results. The highly porous surface and large sized cavity observed in Fig. 1(e) confirm the presence of the tensile residual stresses for 500 pulses. Refilling of the cavities and cracks with shock liquefied material results in the compressive stresses for 1000 pulses (Fig. 1(f)). Further increase in laser pulses to 2000 again results in enhanced densities of pores, cavities, and cracks (Fig. 1(h)), which is evident for the presence of highly tensile stresses.

Figure 4(a) shows the XRD patterns of the pristine and the laser irradiated zirconium exposed to various numbers of laser pulses under an ambient environment of propanol. New phases of zirconium oxide (tetragonal): ZrO_2 (102), (114); monoclinic: ZrO_2 (-111), (212) and zirconium hydride: ZrH (122), (004), and (110) are observed along with the original phases of zirconium. Figure 4(b) shows the variation in the crystallite size of ZrO_2 (102) plane reflection as a function of laser pulses and figure 4(c) presents the variation in the residual stresses with an increasing number of laser pulses.

A continuous decrease in the peak intensity and the crystallite size is observed with an increase in the number of laser pulses up to 2000. For 500 laser pulses, the tensile stresses are dominant, which relax with an increase in the number of laser pulses up to 2000. The peak shifting to a higher angular position is also evident for the transformation of tensile to compressive residual stresses. Melting of the target during the laser irradiation activates a reaction between the oxygen/hydrogen and the molten surface. During the recrystallization process, oxygen/hydrogen diffuses into the surface, which causes a reduction in the crystallite size and the tensile stresses to relax.[40] The relaxation of the tensile residual stresses could also be due to an annealing effect after increasing multiple laser-irradiations. The defects and stresses produced by the initial pulses are annealed and relaxed after successive pulses.[41] These results are well correlated with the

change in the surface morphology (Figs. 2(e)–2(h)). A decrease in the size of nanopores, cracks, and nanocavites due to refilling by the melted material is attributable to the continuous decrease in the tensile residual stresses.
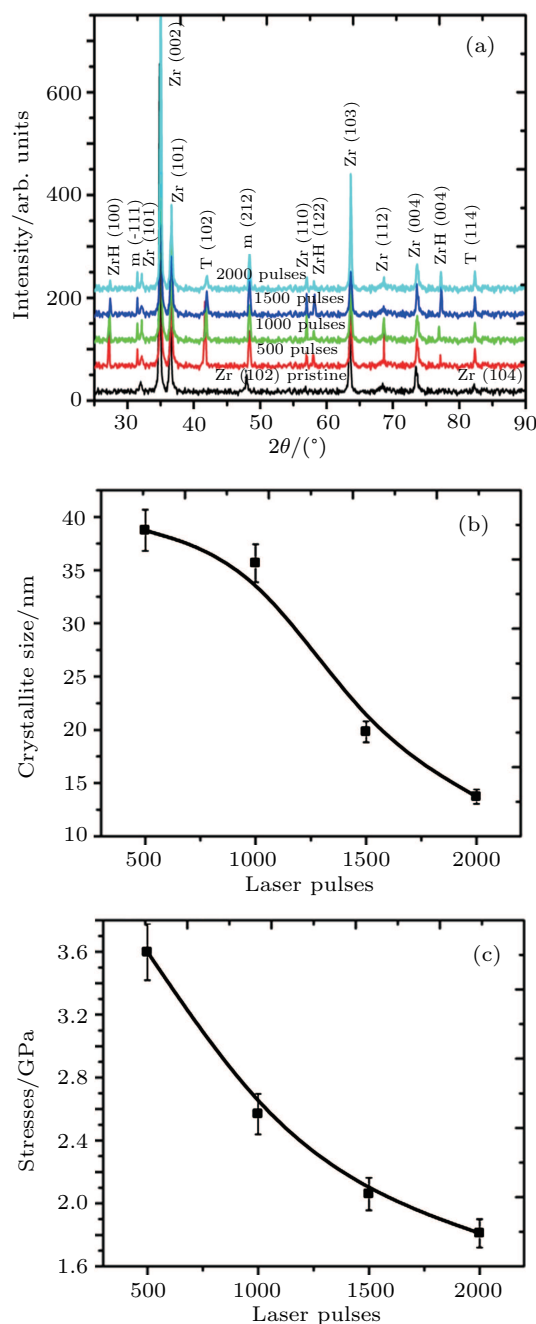

Fig. 4. (color online) (a) XRD patterns of the pristine and the femtosecond laser irradiated zirconium exposed to various numbers of laser pulses at a fixed fluence of 3.6 J/cm² under an ambient environment of propanol. (b) The variation in the crystallite size and (c) the variation in stresses for varying pulses.

A comparison of the XRD results of both media shows similarities in the chemical structure of the surface. The irradiated zirconium shows the formation of a mixture of monoclinic and tetragonal phases of zirconia for both ambient environments along with various phases of zirconium hydride. However excessive hydrides are formed in the case of propanol

only.

Figure 5(a) presents the Raman spectrum of zirconium irradiated at a fluence of 3.6 J/cm^2 in an ambient environment of propanol for 1000 laser pulses. The Raman peaks identified at 176 cm^{-1}, 223 cm^{-1}, 344 cm^{-1}, 474 cm^{-1}, 500 cm^{-1}, 569 cm^{-1}, 640 cm^{-1}, and 725 cm^{-1} represent the monoclinic phase of ZrO_2, whereas the peak observed at 315 cm^{-1} can be assigned as the characteristic of the tetragonal phase of ZrO_2.[42,43] The peak observed at 832 cm^{-1} is the characteristic of the metal–hydroxide (M–OH) M–O streching mode.[44]

Figure 5(b) presents the Raman spectrum of zirconium irradiated at a fluence of 3.6 J/cm^2 in an ambient environment of de-ionized water for 1000 laser pulses. The Raman peaks identified at 149 cm^{-1}, 315 cm^{-1}, 456 cm^{-1} represent the tetragonal phase of ZrO_2, while the Raman peaks observed at 190 cm^{-1}, 223 cm^{-1}, 380 cm^{-1}, 615 cm^{-1}, and 725 cm^{-1} can be assigned as the characteristic of the monoclinic phase of ZrO_2.[42] One Raman peak is identified at 607 cm^{-1}, which represents the cubic phase of ZrO_2, while the peak observed at 403 cm^{-1} can be considered as the characteristics of metal–hydroxide (M–OH).[13]
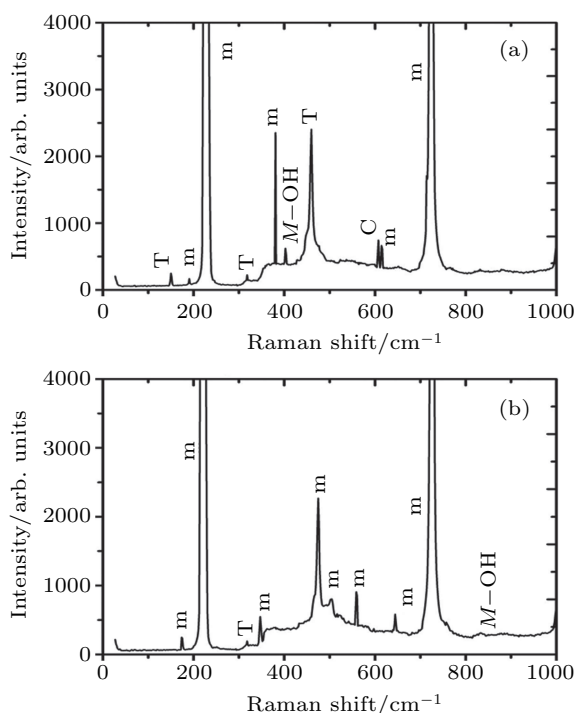

Fig. 5. Raman spectra of the zirconium targets exposed to 1000 femtosecond laser pulses at a fluence of 3.6 J/cm^2 in ambient environments of (a) de-ionized water and (b) propanol (m represents monoclinic and T represents tetragonal phase of zirconium oxide ZrO_2).

A comparison of both media shows dissimilarities in the chemical structure of the surface. The irradiated zirconium shows the formation of a mixture of monoclinic and tetragonal phases of zirconia for both ambient environments, whereas cubic zirconia is formed only in the case of de-ionized water. The formation of zirconium hydride is also evident in both

environments. Similar results are seen during XRD analysis, which confirms the formation of both monoclinc and tetragonal phases of zirconia for both environments along with the formation of hydrides of zirconium. The formation of cubic zirconia is also observed in the case of de-ionized water.

Pulsed laser ablation in liquid is an extremely non-equilibrium process. When the target is irradiated by femtosecond laser pulses, the ejected species will have large kinetic energy after irradiation and a plasma plume will be formed at the interface. The plasma plume expands adiabatically while the liquid confines itself. The confinement effect of the liquid results in the plasma plume changing into a more high thermodynamic state in which the pressure and temperature increase significantly.[45] The plume species collide and react with the surrounding liquid molecules and preferentially form the metastable materials in these extreme states. Moreover, the cooling effects of the liquid can cause quenching of the plasma plume, which solidifies and preserves the metastable materials in the final yield. In our case, at room temperature, tetragonal and cubic phases of zirconium oxide (ZrO_2) are metastable. The ablated species from the target react with the molecules of the surrounding liquid at high temperature and pressure. After fast quenching of the plasma plume, tetragonal and cubic zirconia nanocrystallites are synthesized and reserved.

Various theories have been proposed for the stabilization of metastable tetragonal and cubic phases in nanocrystalline zirconia at room temperature. Many researchers presented that oxygen vacancies play a significant role in the stabilization of nanocrystalline tetragonal and cubic zirconia at room temperature.[46] The above results describe how femtosecond pulsed laser ablation in liquids is favorable for the synthesis and stabilization of metastable zirconia and ZrH.

The untreated zirconium sample shows a nanohardness of 0.85 GPa. Figure 6 shows the variation in the nanohardness of the femtosecond laser irradiated zirconium targets as a function of increasing the number of laser pulses. Figure 6(a) shows the variation in the nanohardness after irradiation in an ambient environment of de-ionized water. For 500 laser pulses, a nanohardness of 0.90 GPa is obtained. An increase in the number of laser pulses up to 1000 leads to an increase in the hardness up to 0.95 GPa. A further increase in the number of laser pulses upto 2000 shows a decrease in the hardness down to 0.86 GPa. Figure 6(b) shows the variation in the hardness after irradiation in an ambient environment of propanol. For 500 laser pulses, a hardness of 0.85 GPa is obtained. Increasing the number of laser pulses up to 2000 shows a continuous increase in the hardness up to 0.96 GPa.

The increase in the hardness is attributable to the interstitial diffusion of oxygen into the lattice, which results in a decrease in the crystallite size and the tensile residual

stresses (Fig. 3(b)).[47] Smaller crystallite size is efficient in obstructing the dislocation movement and is responsible for high strength and hardness. This increase in the hardness depends on a number of factors including the lattice defects, density of oxide contents, phase composition, size and distribution of grain, and crystal structure.[48] These results can be verified by using the Hall–Petch relationship[49]

$$H = H_{\mathrm{o}} + K_{\mathrm{H}}(d)^{-1/2},$$

where H_{o} and K_{H} are experimental constants, d is the average grain size, and H is the hardness.
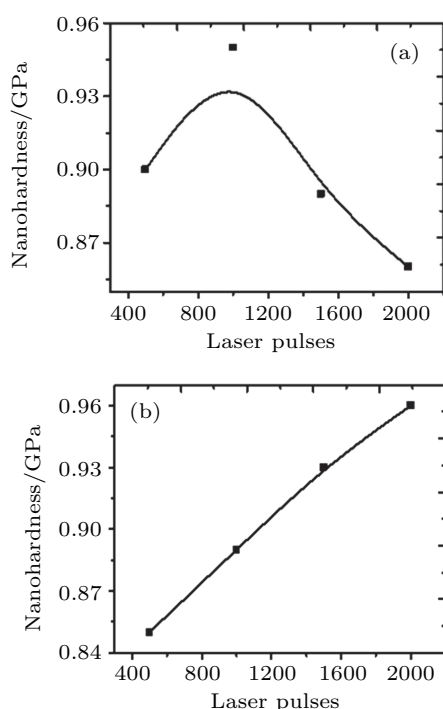

Fig. 6. The variation in nanohardness of laser treated zirconium in ambient environments of (a) de-ionized water and (b) propanol.

The decrease in the hardness of the irradiated zirconium targets in the de-ionized water environment can be explained on the basis of the enhanced tensile residual stresses. Oxygen diffusion across the grain boundaries results in larger crystallites (Fig. 3(b)) that are more prone to coarsening, leading to lower crystallite density and hence lower hardness.[47]

4. Conclusions

Femtosecond pulsed laser ablation performance of zirconium in de-ionized water and propanol environments has been investigated. The results suggest that the ambient environment plays a significant role in surface and structural modification of zirconium. The surface morphologies of the craters produced in de-ionized water are much smoother than those produced in propanol, which might be due to the different interacting mechanisms, such as recoil pressures, absorption coefficients, production of bubbles, etc. In the case of ablation in de-ionized water, LIPSS are observed at both the central and the peripheral ablated areas along with some bifurcations such as pores, cavities, and cracks. While, in the case of a propanol environment, a sponge like surface structure, cones, cracks, and cavities are seen at the central ablated area. The peripheral ablated area shows only flake like structures and cracks. No LIPSS are seen after irradiation in propanol. These results confirm that de-ionized water is more supportive for the growth of LIPSS. The formation of the above mentioned surface structures may be attributed to various mechanisms, such as interference, hydrodynamic instability, self-organization process, and explosive boiling. EDS analysis confirms the increase in the content of oxygen in both ambient environments. XRD and Raman analyses confirm the presence of various phases of titanium oxide during ablation in both ambient environments. The presence of different phases of hydrides is also evident for both environments. Convective bubble motion and pressure gradients owing to the confinement effects of liquids along with the development of a variety of oxides and hydrides are accountable for the generation of these small scale structures. The reduced energy deposition due to shielding effects and fast cooling makes the liquid ablation a more effective tool for the nano-structuring of the materials. The variation in crystallite size is responsible for the variation in nanohardenss of the irradiated samples and can be well explained on the basis of the Hall Petch relationship.

Acknowledgment

References

[1] Dauscher A, Feregotto V, Cordier P and Thorny A 1996 *Appl. Surf. Sci.* **96–98** 410
[2] Karimzadeh R, Anvari J Z and Mansour N 2009 *Appl. Phy. A* **94** 949
[3] Giron A G, Sola D and Peña J I 2016 *Appl. Surf. Sci.* **363** 548
[4] Kanitz A, Hoppius J S, Gurevich E L and Ostendorf A 2016 *Phys. Procedia* **83** 114
[5] Umm-i Kalsoom, Bashir S and Ali N 2013 *Surf. Coat. Technol.* **235** 297
[6] Gurevich E L 2016 *Appl. Surf. Sci.* **374** 56
[7] Bashir S, Rafique M S, Nathala C S and Husinsky W 2014 *Appl. Surf. Sci.* **290** 53
[8] Root R G 1989 *Laser-Induced Plasmas and Applications* (New York: Marcel Dekker)
[9] Speight J 1952 *Lange's Handbook of Chemistry* (16th Edn.) (New York: McGraw-Hill Education)
[10] Murtaza G, Hussain S S, Rehman N U, Naseer S, Shafiq M and Zakaullah M 2011 *Surf. Coat. Technol.* **205** 3012

[11] Barmina E V, Serkov A A, Stratakis E, Fotakis C, Stolyarov V N, Stolyarov I N and Shafeev G A 2012 *Appl. Phys. A* **106** 1

[12] Vorobyev A Y and Guo C 2005 *Phys. Rev. B* **72** 195422

[13] Tan D, Lin G, Liu Y, Teng Y, Zhuang Y, Zhu B, Zhao Q and Qiu J 2011 *J. Nanopart. Resear.* **13** 1183

[14] Li M, Feng Z, Xiong G, Ying P, Xin Q and Li C 2001 *J. Phys. Chem.* **105** 8107

[15] Huston E L and Sandrock G D 1980 *J. Less Comm. Metal.* **74** 435

[16] Evans D G and Duan X 2006 *Chem. Commun.* **485–496** 485

[17] Ali N, Bashir S, Umm-i-Kalsoom, Akram M and Mahmood K 2013 *Appl. Surf. Sci.* **270** 49

[18] Asibu-Jr E K 2009 *Principals of Lasers Materials Processing* (New Jersey: Wiley)

[19] Bonse J, Rosenfeld A and Küger J 2009 *J. Appl. Phys.* **106** 104910

[20] bandoki P B, Valette S, Audouard E and Benayoun S 2013 *Appl. Surf. Sci.* **270** 197

[21] Bonse J, Hohm S, Rosenfeld A and Kruger J 2013 *Appl. Phys. A* **110** 547

[22] Kim S H, Sohn I B and Jeong S 2011 *Appl. Phys. A* **103** 1053

[23] Murphy R D, Torralva B, Adams D P and Yalisove S M 2013 *Appl. Phys. Lett.* **102** 211101

[24] Ionin A A, Kudryashov S I, Makarov S V, Rudemko A A, Seleznev L V, Sinitsyn D V, Golosov E V, Kolobov Y R and Ligachev A E 2012 *Appl. Phys. A* **107** 301

[25] Furusawa K, Takahashi K, Cho S H, Kumagai H, Midorikawa K and Obara M 2000 *J. Appl. Phys.* **87** 1604

[26] Park H K, Grigoropoulos D P, Poon C C and Tam A C 1996 *Appl. Phys. Lett.* **68** 596

[27] Geohegan D B, Puretzky A A, Duscher G and Pennycook S J 1998 *Appl. Phys. Lett.* **72** 2987

[28] Romashevskiy S A, Ashitkov S I, Ovchinnikov A V, Kondratenko P S and Agranat M B 2016 *Appl. Surf. Sci.* **374** 12

[29] Umm-i-Kalsoom, Bashir S, Ali N, Akram M, Mahmood K and Ahmad R 2012 *Appl. Surf. Sci.* **261** 101

[30] Mansour N, Ghaleh K J and Ashkenasi D 2006 *J. Laser Micro/Nanoengineer.* **1** 12

[31] Shen M Y, Crouch C H, Carey J E and Mazur E 2004 *Appl. Phys. Lett.* **85** 5694

[32] Raillard L G B, Moore E R, Grandthyll S, Müller F and Mücklich F 2012 *Surf. Coat. Technol.* **207** 102

[33] Ashraf M, Akhtar S M J, Khan A F, Ali Z and Qayyum A 2011 *J. Alloy. Compd.* **509** 2414

[34] http://www.memsnet.org/material/zirconiumoxidezro2/

[35] Latif A, Rehman M K, Rafique M S and Bhatti K A 2011 *Physica B* **406** 1713

[36] Khan I A, Hassan M, Ahmad R, Qayyum A, Murtaza G, Zakaullah M and Rawat R S 2008 *Thin Solid Film.* **516** 8255

[37] Gurarie V N, Otsuka P H, Jamieson D N and Prawe S 2006 *Nucl. Instr. Meth. Phys. Resear. B* **242** 421

[38] Onge L S, Sabsabi M and Cielo P 1998 *Spectrochimica Acta B* **53** 407

[39] Mahmood K, Farid N, Ghauri I M, Afzal N, Idrees Y and Mubarik F E 2010 *Physica Scripta* **82** 045606

[40] Umm-i-Kalsoom, Bashir S and Ali N 2013 *Surf. Coat. Technol.* **235** 297

[41] Rafique M S, Rehman M K, Firdos T, Aslam K, Anwar M S, Imran M and Latif H 2007 *Laser Phys.* **17** 1138

[42] Barberis P, Mrjean T M and Quintard P 1997 *J. Nucl. Mater.* **246** 232

[43] Zhang W, Gan J, Hu Z, Yu W, Li Q, Sun J, Xu N, Jiadawu and Ying Z 2011 *Appl. Spectr.* **65** 522

[44] Socrates G 2001 *Infrared and Raman Characteristic Group Frequencies: Tables and Charts* (3rd Edn.) (Chichester: Wiley)

[45] Amendola V and Meneghetti M 2009 *Phys. Chem. Chem. Phys.* **11** 3805

[46] Shukla S and Seal S 2005 *Inter. Mater. Rev.* **50** 45

[47] Umm-i-Kalsoom, Ahmad R, Ali N, Khan I A, Saleem S, Ikhlaq U and Khan N 2013 *Plasma Sci. Technol.* **15** 666

[48] Warcholinski B and Gilewicz A 2009 *J. Achiev. Mater. Manuf. Eng.* **37** 498

[49] Lim Y Y and Chaudhri M M 2002 *Philos. Mag. A* **82** 2071